Electronic Supplementary Material (ESI) for Inorganic Chemistry Frontiers.
This journal is © the Partner Organisations 2020

Electronic Supporting Information (ESI)

Construction of a Novel Nickel-based MOF with Accessible Oxygen Sites for Efficient CH_4/N_2 Separation†

*Feifei Zhang[a], Yuhao Tang[a], Zhiwei Zhao[a], Mengyue Lu[a], Xiaoqing Wang[a,b], Jinping Li[a,b] and Jiangfeng Yang[a,b,]**

[a] Research Institute of Special Chemicals, College of Chemistry and Chemical Engineering, Taiyuan University of Technology, Taiyuan 030024, Shanxi, China.

[b] Shanxi Key Laboratory of Gas Energy Efficient and Clean Utilization, Taiyuan 030024, Shanxi, China.

*Corresponding author: E-mail: yangjiangfeng@tyut.edu.cn;

Experimental Section

1. Sample preparation

Preparation of TUTJ-201Co single crystals: $Co(NO_3)_2 \cdot 3H_2O$ (90.0 mg, 0.37 mmol) and H_2L (30.0 mg, 0.12 mmol) were added to a 20 mL glass vial, and then, 9.0 mL of DMA, 0.9 mL of H_2O, and 1.3 mL of HBF_4 (48 wt %) were added to the glass vial by using a pipette. The vial was sealed and placed in an oven. The oven temperature was increased from room temperature to 353 K within 1 h and kept at this temperature for 24 h. Then, the reaction kettle was taken out of the oven and naturally cooled to the room temperature. The products were collected by suction filtration and washed several times with fresh DMA and acetone.

2. Single-crystal X-ray diffraction studies

Crystallographic data of TUTJ-201Co was collected on XtaLAB Synergy which was equipped with single source at home/near Cu X-ray sources (λ = 1.5405 Å) at 100 K. The structures were solved with dual-direct methods using SHELXTL and refined with the full-matrix least-squares technique based on F2 using the SHELXL-2014 program package and Olex-2 software. Non-hydrogen atoms were refined anisotropically, and all hydrogen atoms bound to C were generated geometrically. The crystal data of these compounds are listed in Table S1. The X-ray crystallographic coordinates for structures reported in this article have been deposited at the Cambridge Crystallographic Data Centre (CCDC) under deposition numbers CCDC 2345232. These data can be obtained free of charge from the Cambridge Crystallographic Data Centre via http://www.ccdc.cam.ac.uk/data_request/cif.

3. Fitting of pure component isotherms

The single-component N_2 and CH_4 adsorption isotherms of TUTJ-201Ni were fitted using the dual-

site Langmuir-Freundlich (DSLF) model, and R^2 was greater than 0.9999.

$$q = q_1 \frac{b_1 P^{1/n_1}}{1 + b_1 P^{1/n_1}} + q_2 \frac{b_2 P^{1/n_2}}{1 + b_2 P^{1/n_2}} \quad (1)$$

Where q is the equilibrium adsorbed amount of an adsorbent (mmol/g); q_1 and q_2 are the saturation uptakes of site 1 and site 2 (mmol/g); b_1 and b_2 are the affinity coefficients of site 1 and site 2 (1/bar); n_1 and n_2 are the corresponding deviations from an ideal homogeneous surface.

4. Q_{st} calculation

The Q_{st} of TUTJ-201Ni with N_2 and CH_4 were calculated using the N_2, CH_4 single-component adsorption isotherms at 273 K and 298 K via the Clausius-Clapeyron equation.

$$In \frac{p_2}{p_1} = \frac{\Delta H}{R} \left(\frac{1}{T_1} - \frac{1}{T_2} \right) \quad (2)$$

In the above equation, P represents the pressure, the unit is bar, T is the temperature in K, and R is the gas constant (8.314).

5. IAST calculations of adsorption selectivity

The two-component gas selectivity calculation formula is defined as:

$$S_{ads} = \frac{q_1 / q_2}{p_1 / p_2} \quad (3)$$

Where, q_1 and q_2 are the absolute adsorption amounts of the components, and p_1 and p_2 are the partial pressures of the components in the gas mixture.

6. Computational method

6.1 Grand Canonical Monte Carlo (GCMC) simulations

The probability distributions of CH_4 and N_2 were simulated at 298 K 1bar by using the Grand Canonical Monte Carlo (GCMC) approach as implemented in the RASPA simulation code.[1] The simulations assumed the MOF to be rigid. The Lennard-Jones parameters was determined by using the Universal Force Field (UFF) for the MOF.[2] N_2 molecule was described using a three-site charged model with two Lennard-Jones sites on the Nitrogen atoms and a central site (center of mass) for purely electrostatic interactions (TraPPE model).[3] CH_4 molecule was treated as unit-atom model (also TraPPE model).[3] Atomic charges for all atoms in the studied MOF were obtained by using the DDEC06 method.[4]

6.2 DFT calculations

Our density functional theory (DFT) calculations[5,6] were carried out in the Vienna *ab initio* simulation package (VASP) based on the plane-wave basis sets with the projector augmented-wave method.[7,8] The exchange-correlation potential was treated by using a generalized gradient approximation (GGA) with the Perdew-Burke-Ernzerhof (PBE) parametrization.[9] The van der Waals correction of Grimme's DFT-D3 model was also adopted.[10] The energy cutoff was set to be 520 eV. The Brillouin-zone integration was sampled with a Γ-centered Monkhorst-Pack mesh of 2 × 1 × 2.[11] The structures were fully relaxed until the maximum force on each atom was less than 0.01 eV/Å, and the energy convergent standard was 10^{-5} eV. The structure was fully relaxed and reached the minimum energy principle during the structure optimization process.

Supporting Table and Figures

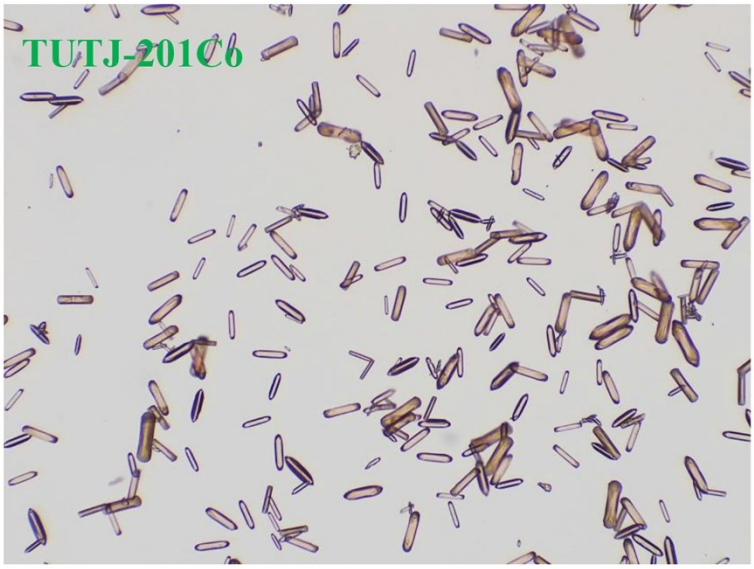

Figure S1. Photograph of the crystals of TUTJ-201Co.

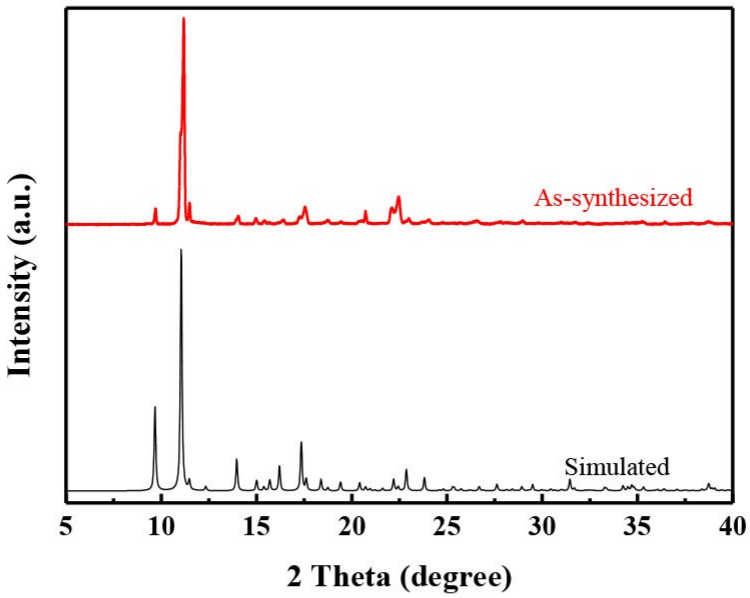

Figure S2. The simulated XRD pattern from the single-crystal X-ray structure of TUTJ-201Co (black), and the PXRD patterns of as-synthesized powder (red) of TUTJ-201Co.

Table S1. Crystallographic parameters of TUTJ-201Co.

Crystal data	TUTJ-201Co
CCDC number	22345232
Empirical formula	$C_{24}H_{12}Co_2N_4O_9$
Formula weight	618.24
Temperature/K	100.00(10)
Crystal system	*orthorhombic*
Space group	*Pbcn*
a / Å	10.3752(4)
b / Å	19.2876(8)
c / Å	14.3402(6)
α/°	90
β/°	90
γ/°	90
Volume/ Å^3	2869.7(2)
Z	4
Density/g/cm^3	1.431
μ/mm $^{-1}$	1.209
F(000)	1240.0
Reflections collected	17211
Independent reflections	3758 [R_{int} = 0.0488, R_{sigma} = 0.0465]
Goodness-of-fit on F^2	1.033
R1a[I>2σ(I)]	R_1 = 0.0399, wR_2 = 0.1134
ωR2b[I>2σ(I)]	R_1 = 0.0535, wR_2 = 0.1197
Largest diff. peak/hole / e Å^{-3}	0.74/-0.49

Table S2. Crystallographic parameters of TUTJ-201Ni.

Crystal data	TUTJ-201Ni
CCDC number	2345233
Empirical formula	$C_{24}H_{12}Ni_2N_4O_9$
Formula weight	617.78
Crystal system	*Orthorhombic*
Space group	*P b c n*
a / Å	10.2897(1)
b / Å	18.6265(5)
c / Å	14.3605(4)
α/°	90
β/°	90
γ/°	90
Rwp	0.0612
Rp	0.0468
GOF	2.01
X_2	4.03

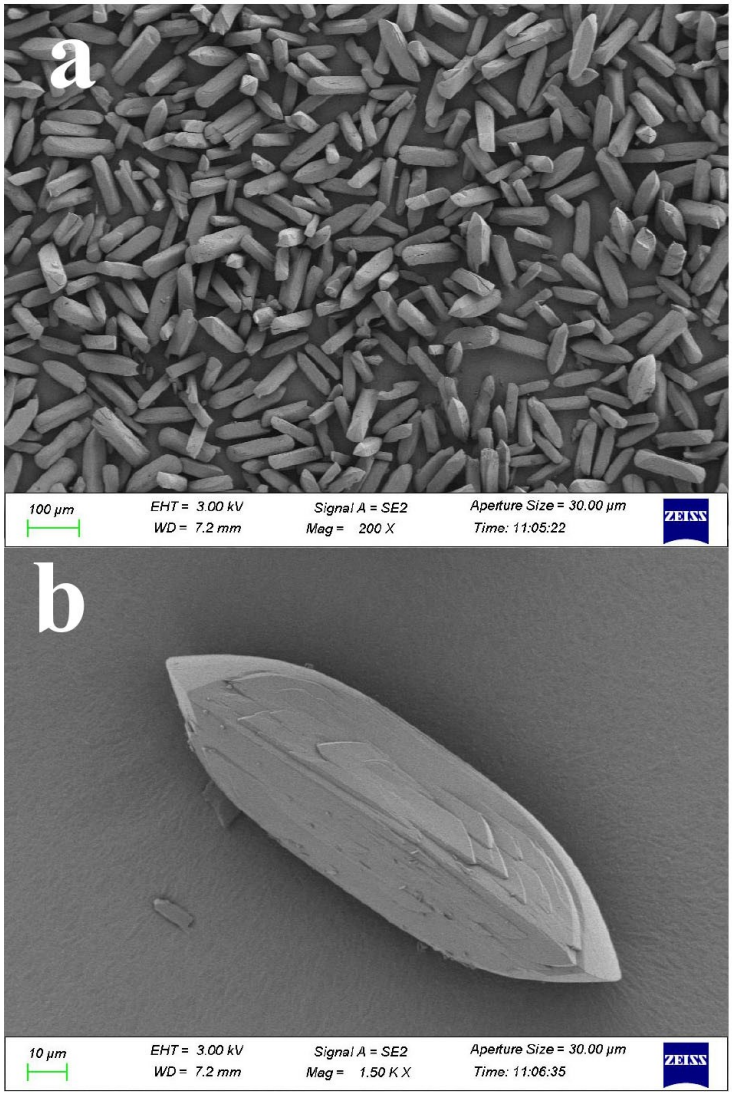

Figure S3. SEM images of as made TUTJ-201Co (a, b).

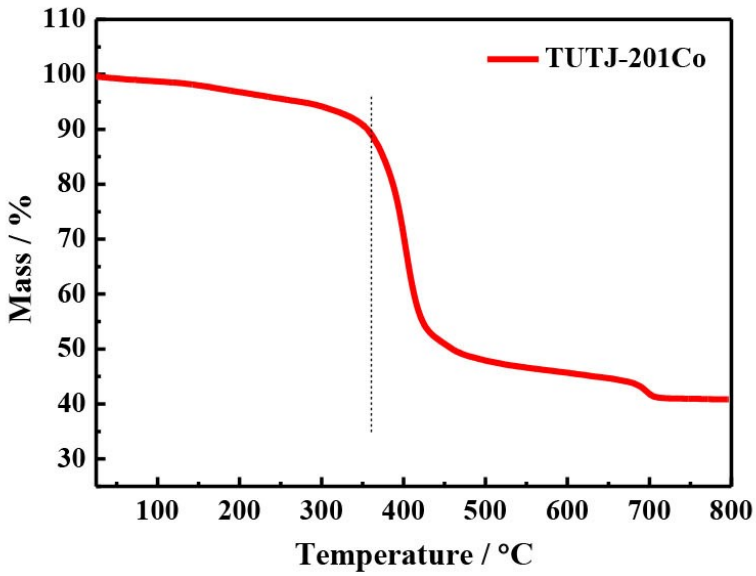

Figure S4. TG curve of TUTJ-201Co.

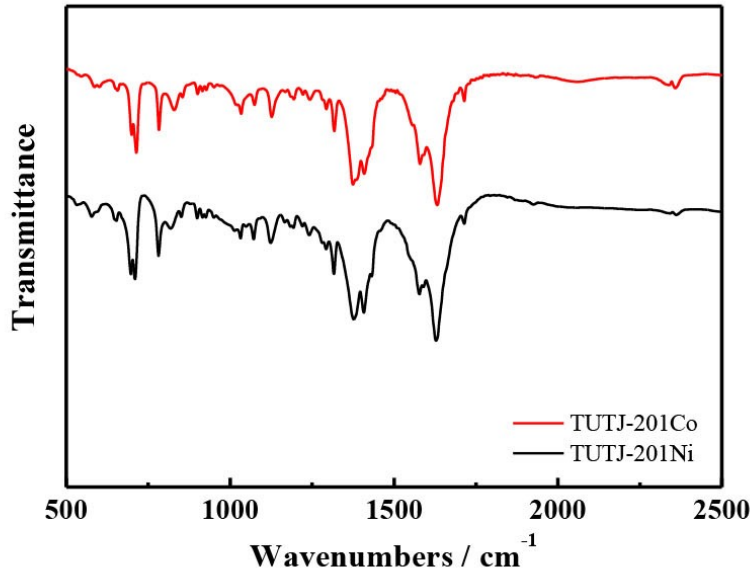

Figure S5. FTIR spectra of TUTJ-201Co and TUTJ-201Ni.

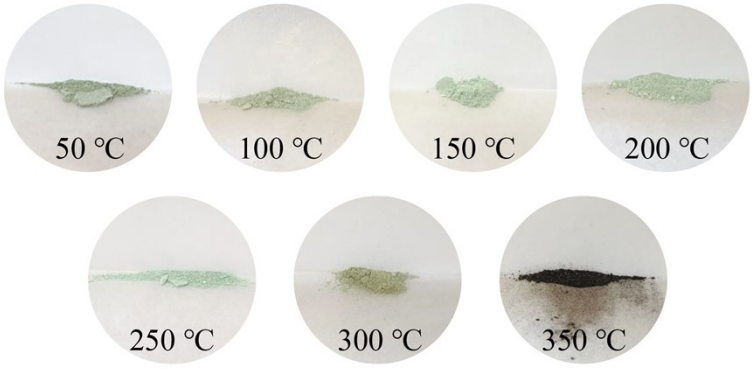

Figure S6. Photographs of TUTJ-201Ni after activation at specific temperatures for 5 h.

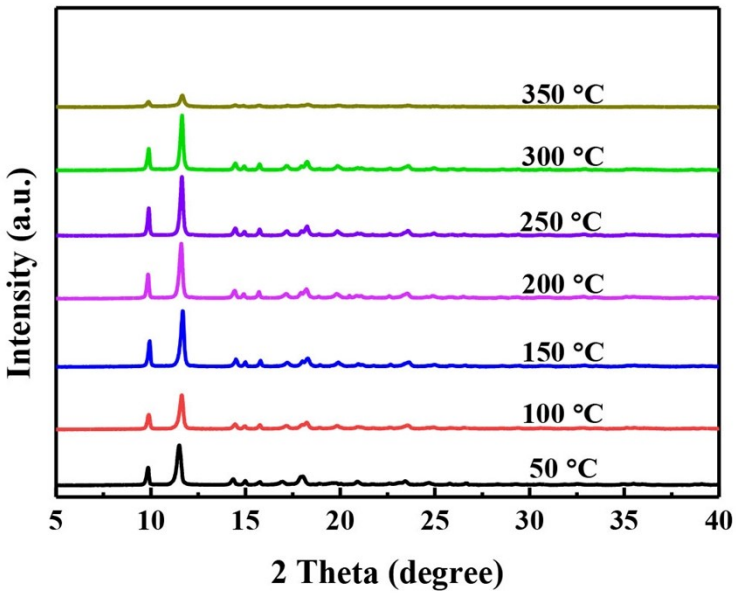

Figure S7. Variable-temperature PXRD patterns for TUTJ-201Ni. Obviously, the crystal structure of TUTJ-201Ni remains stable under the degassing conditions of 300 ºC, indicating its highly thermal stability.

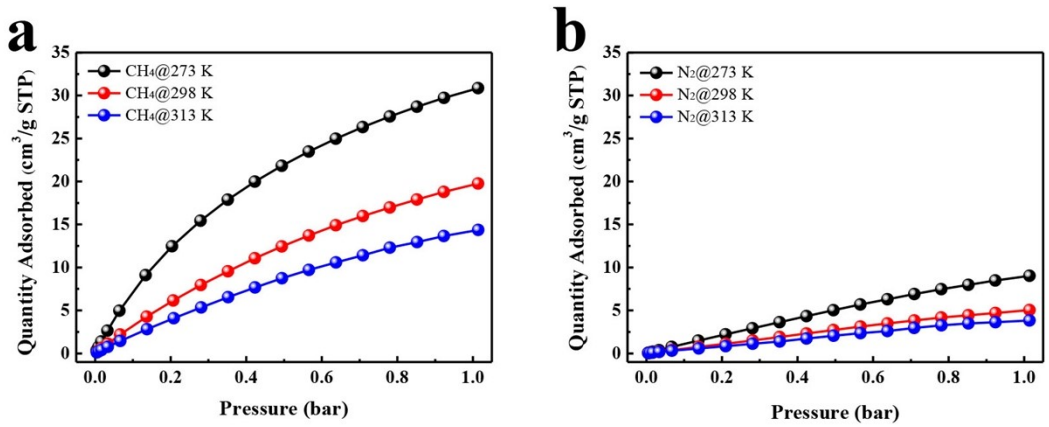

Figure S8. N_2, CH_4 single-component adsorption isotherms at 273, 298 and 313 K, which used for the calculation of isosteric heats by using the Clausius-Clapeyron equation.

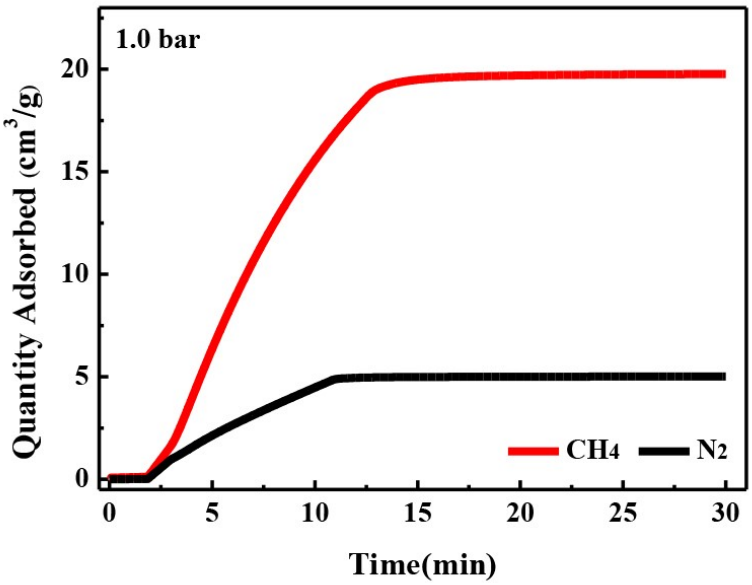

Figure S9. Kinetic adsorption curves for CH_4 and N_2 at 1.0 bar and 298 K. The slope of kinetic adsorption curve of CH_4 is notably higher than that of N_2, indicating a faster CH_4 adsorption rate.

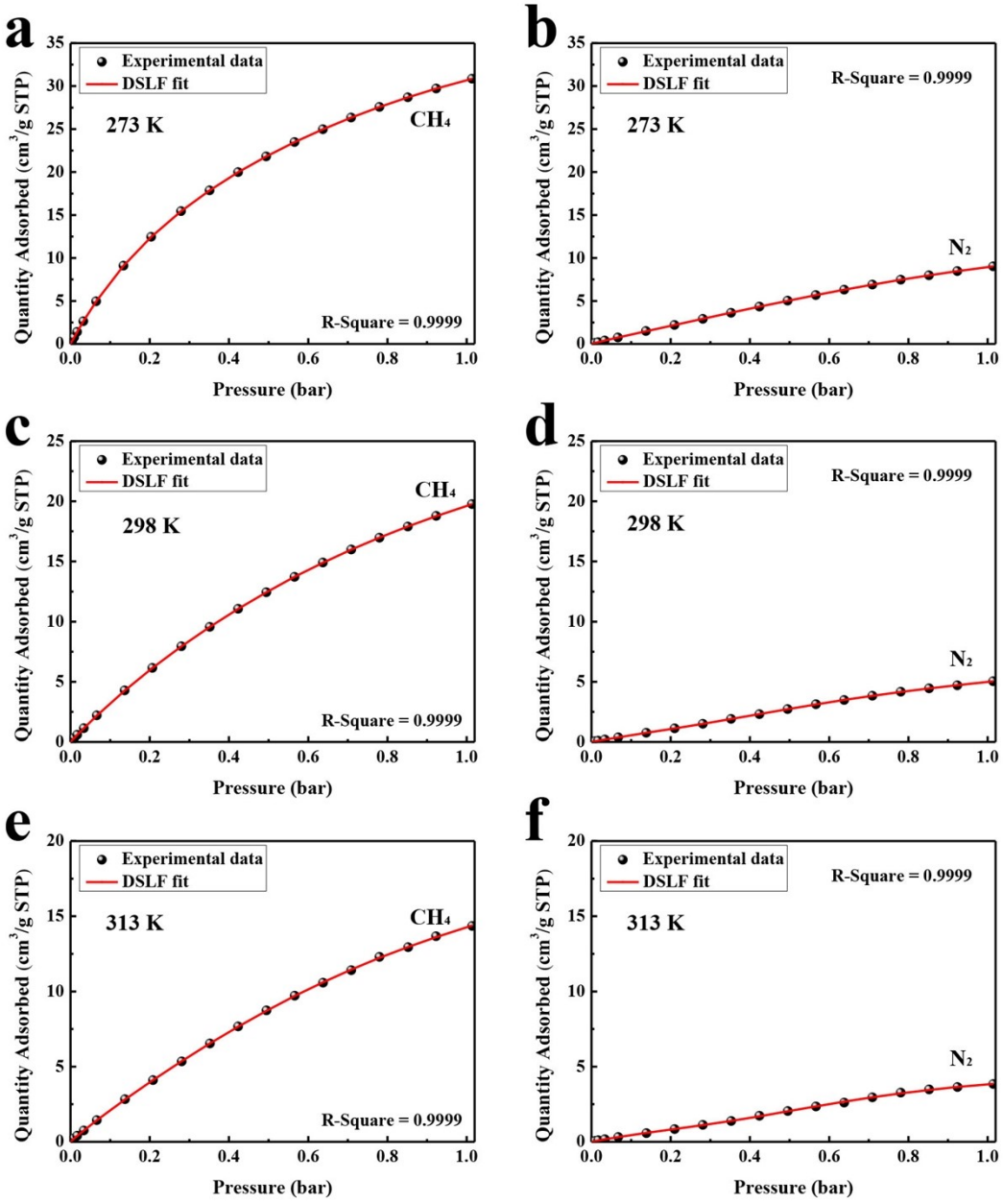

Figure S10. N_2 and CH_4 adsorption isotherms at 273, 298 and 313 K in TUTJ-201Ni with dual-site Langmuir-Freundlich model fits.

Table S3. Test conditions and DSLF fit parameters for CH_4 and N_2 in TUTJ-201Ni of **Figure S10.**

Numbering	**T. T.**[a]	q_1	b_1	n_1	q_2	b_2	n_2
(a)	273	3.39E1	2.73	0.98	1.16E1	1.02	0.52
(b)	273	1.09E1	1.13	0.53	4.22	2.90	0.99
(c)	298	4.31E1	0.79	1.00	0.55	1.03E1	0.26
(d)	298	1.81E1	0.30	1.02	0.89	8.98	0.27
(e)	313	1.61E1	1.19	0.60	7.55	2.67	1.03
(f)	313	2.38	3.40	0.31	3.38	1.41	1.02

[a]: “T. T.” stands for test temperature, the unit is “K”.

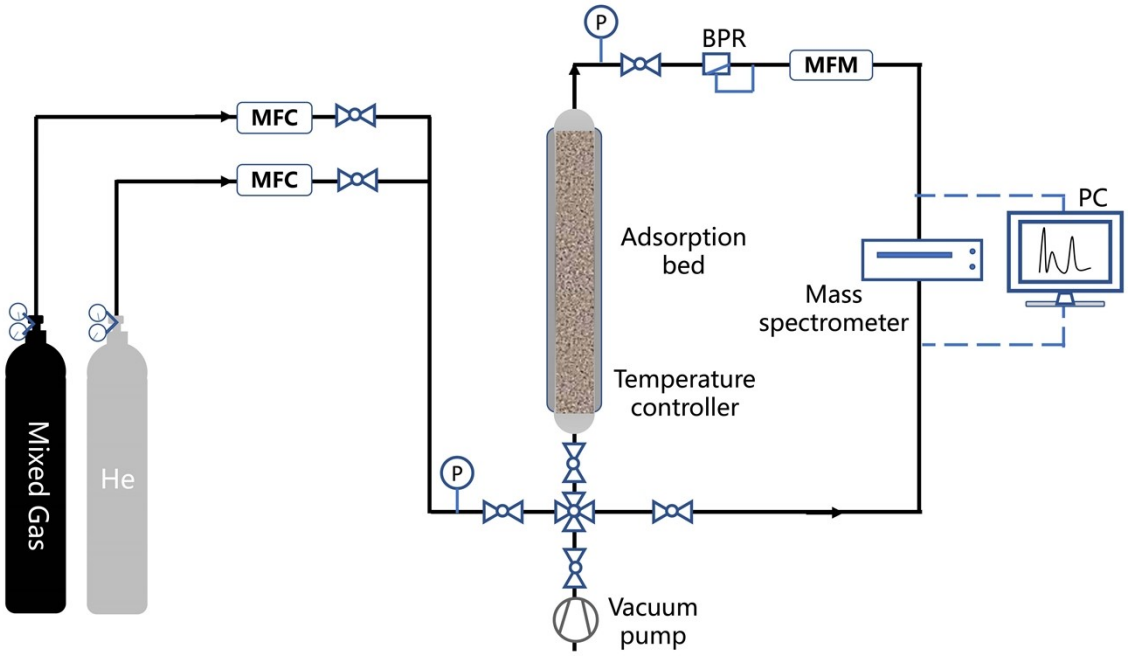

Figure S11. Schematic illustration of home-built rig for gas breakthrough experiment.

Table S4 Atomic content in TUTJ-201Ni

Names	Atomic %				O/Ni Atomic ratio
	Ni2p	C1s	O1s	N1s	
TUTJ-201Ni	5.06	60.1	24.54	10.3	4.85

Note: Atomic content was evaluated by a multifunctional X-ray photoelectron spectrometer (Thermo ESCALAB 250XI).

Table S5. Comparison of adsorptive separation properties of TUTJ-201Ni with the selected various porous materials reported in the literature.

Sample	**50/50 CH_4/N_2 selectivity**	**CH_4 uptake (cm^3/g) 298 K**	**N_2 uptake (cm^3/g) 298 K**	**CH_4 Q_{st} (kJ/mol)**	**Ref.**
$Ni(ina)_2$	15.8	46.7	14.5	28.0	12
Al-CDC	13.1	32.0	5.1	27.5	13
$Co_3(C_4O_4)_2(OH)_2$	12.5	8.9	4.1	25.1	14
CAU-21-BPDC	11.9	22.2	4.2	20.5	15
SBMOF-1	11.5	20.6	4.0	23.5	16
ATC-Cu	9.7	64.9	16.8	26.8	17
STAM-1	10.8	14.2	2.4	20.0	13
NKMOF-8-Me	9.0	39.5	7.0	28.0	18
MIL-160	8.9	10.5	3.0	10.7	19
ClCTF-1-650	8.6	32.9	7.8	22.0	20
Al-FUM-Me	8.6	27.2	5.0	24.1	21
MOF-888	8.4	10.0	1.8	26.0	22
$Cu(INA)_2$	8.3	18.6	2.7	17.5	23
MOF-891	7.8	30.0	6.4	22.0	22
ZIF-94	7.4	33.6	8.2	23.9	24
Ni-Qc-5-Dia	7.4	29.3	6.2	19.5	25
Ni-MA-BPY	7.4	22.6	4.7	23.5	26

Ni(BTC)(PIZ)	7.3	36.3	7.8	18.1	27
Co-MA-BPY	7.2	20.6	4.4	22.8	26
DMOF-A_2	7.2	37.0	8.8	22.5	28
CAU-10	7.2	16.6	5.3	7.1	19
$Ni(OAc)_2L$	7.0	25.7	10.5	26.7	29
MOF-890	7.0	24.0	6.0	23.0	22
$Cu(hfipbb)(H_2hfipbb)_{0.5}$	6.9	10.5	2.9	24.0	30
MOF-889	6.4	26.0	5.3	22.0	22
TUT-100	6.3	27.5	5.0	23.7	31
$[Ni_3(HCOO)_6]$	6.2	18.4	4.0		32
$[Co_3(HCOO)_6]$	5.1	11.0	2.7	23.0	33
UiO-66-Br_2	5.1	16.1	4.4		34
PAF-26-COOH	4.2	12.1	3.0	14.0	35
MOF-177	4.0	12.5	3.0	11.7	36
MIL-53(Al)	3.7	16.6	5.0	19.0	37
Al-BDC	3.6	16.4	5.0	18.7	23
ZIF-93	3.6	11.7	3.6	15.8	24
NU-1000	2.5	10.8	4.4		38
ZIF-8	2.5	7.8	2.0	17.0	24
MIL-120Al	6.0	33.7	10.5	20.9	39
TUTJ-201Ni	**7.2**	**19.8**	**5.0**	**24.5**	**This work**

References

[1] Dubbeldam, D.; Calero, S.; Ellis, D. E.; Snurr, R. Q. RASPA: Molecular Simulation Software for Adsorption and Diffusion in Flexible Nanoporous Materials, *Mol. Simul.,* 2016, **42**, 81-101.

[2] Rappe, A. K.; Casewit, C. J.; Colwell, K. S.; Goddard, W. A.; Skiff, W. M. A Full Periodic Table Force Field for Molecular Mechanics and Molecular Dynamics Simulations, *J. Am. Chem. Soc.,* 1992, **114**, 10024.

[3] Martin, M. G.; Siepmann, J. I. Transferable Potentials for Phase Equilibria. 1. United-Atom Description of n - Alkanes, *J. Phys. Chem. B,* 1998, **102**, 2569-2577.

[4] Manz, T. A.; Limas, N. G. Introducing DDEC6 Atomic Population Analysis: Part 1. Charge Partitioning Theory and Methodology, *RSC Adv.,* 2016, **6**, 47771-47801.

[5] Hohenberg, P.; Kohn, W. Density functional theory (DFT), *Phys. Rev.,* 1964, 136, B864.

[6] Kohn, W.; Sham, L. J. Self-consistent equations including exchange and correlation effects, *Phys. Rev.,* 1965, **140**, A1133-A1138.

[7] Blöchl, P. E. Projector augmented-wave method, *Phys. Rev. B: Condens. Matter Mater. Phys.,* 1994, **50**, 17953.

[8] Kresse, G.; Furthmüller, J. Efficient iterative schemes for ab initio total-energy calculations using a plane-wave basis set, *Phys. Rev. B: Condens. Matter Mater. Phys.,* 1996, **54**, 11169-11186.

[9] Perdew, J. P.; Burke, K.; Ernzerhof, M. Generalized gradient approximation made simple, *Phys. Rev. Lett.,* 1996, **77**, 3865.

[10] Grimme, S.; Antony, J.; Ehrlich, S.; Krieg, H. A consistent and accurate ab initio parametrization of density functional dispersion correction (DFT-D) for the 94 elements H-Pu, *J. Chem. Phys.,* 2010, **132**, 154104.

[11] Monkhorst, H. J.; Pack, J. D. Special points for Brillouin-zone integrations, *Phys. Rev. B,* 1976, **13**, 5188-5192.

[12] Wang, S.-M.; Shivanna, M.; Yang, Q.-Y. Nickel-Based Metal-Organic Frameworks for Coal-Bed Methane Purification with Record CH_4/N_2 Selectivity, *Angew. Chem. Int. Ed.,* 2022, **61**, e202201017.

[13] Chang, M.; Zhao, Y.; Yang, Q.; Liu, D. Microporous Metal-Organic Frameworks with Hydrophilic and Hydrophobic Pores for Efficient Separation of CH_4/N_2 Mixture, *ACS Omega,* 2019, **4**, 14511-14516.

[14] Li, L.; Yang, L.; Wang, J.; Zhang, Z.; Yang, Q.; Yang, Y.; Ren, Q.; Bao, Z. Highly efficient separation of methane from nitrogen on a squarate-based metal-organic framework, *AIChE J.,* 2018, **64**, 3681-3689.

[15] Lv, D.; Wu, Y.; Chen, J.; Tu, Y.; Yuan, Y.; Wu, H.; Chen, Y.; Liu, B.; Xi, H.; Li, Z.; Xia, Q. Improving CH_4/N_2 selectivity within isomeric Al-based MOFs for the highly selective capture of coal-mine methane, *AIChE J.,* 2020, **66**, e16287.

[16] Chang, M.; Ren, J.; Yang, Q.; Liu, D. A robust calcium-based microporous metal-organic framework for efficient CH_4/N_2 separation, *Chem. Eng. J.,* 2021, **408**, 127294.

[17] Niu, Z.; Cui, X.; Pham, T.; Lan, P. C.; Xing, H.; Forrest, K. A.; Wojtas, L.; Space, B.; Ma, S. A Metal-Organic Framework Based Methane Nano-trap for the Capture of Coal-Mine Methane, *Angew. Chem. Int. Ed.,* 2019, **58**, 10138-10141.

[18] Chang, M.; Wang, F.; Wei, Y.; Yang, Q.; Wang, J.-X.; Liu, D.; Chen, J.-F. Separation of CH_4/N_2 by an ultra-stable metal-organic framework with the highest breakthrough selectivity, *AIChE J.,* 2022, **68**, e17794.

[19] Huang, Z.; Hu, P.; Liu, J.; Shen, F.; Zhang, Y.; Chai, K.; Ying, Y.; Kang, C.; Zhang, Z.; Ji, H. Enhancing CH_4/N_2 separation performance within aluminum-based Metal-Organic Frameworks: Influence of the pore structure and linker polarity, *Sep. Purif. Technol.,* 2022, **286**, 120446.

[20] Yao, K. X.; Chen, Y. L.; Lu, Y.; Zhao, Y. F.; Ding, Y. Ultramicroporous carbon with extremely narrow pore distribution and very high nitrogen doping for efficient methane mixture gasesupgrading, *Carbon,* 2017, **122**, 258-265.

[21] Chang, M.; Yan, T.; Wei, Y.; Wang, J.-X.; Liu, D.; Chen, J.-F. Enhancing CH4 Capture from Coalbed Methane through Tuning van der Waals Affinity within Isoreticular Al-Based MOFs, *ACS Appl. Mater. Interfaces.,* 2022, **14**, 25374-25384.

[22] Phuong, T. K. N.; Huong, T. D. N.; Hung, Q. P.; Kim, J.; Kyle, E. C.; Furukawa, H. Synthesis and Selective CO_2 Capture Properties of a Series of Hexatopic Linker-Based Metal-Organic Frameworks, *Inorg. Chem.,* 2015, **54**, 10065-10072.

[23] Hu, J.; Sun, T.; Liu, X.; Guo, Y.; Wang, S. Separation of CH_4/N_2 mixtures in metal-organic frameworks with 1D micro-channels, *RSC Adv.,* 2016, **6**, 64039-64046.

[24] 34. Shi, Q.; Wang, J.; Shang, H.; Bai, H.; Zhao, Y.; Yang, J.; Dong, J.; Li, J. Effective CH_4 enrichment from N_2 by SIM-1 via a strong adsorption potential SOD cage, *Sep. Purif. Technol.,* 2020, **230**, 115850.

[25] Qadir, S.; Gu, Y.; Ali, S.; Li, D.; Zhao, S.; Wang, S.; Xu, H.; Wang, S. A Thermally Stable Isoquinoline Based Ultra-Microporous Metal–Organic Framework for CH_4 Separation from Coal Mine Methane, *Chem. Eng. J.,* 2022, **428**, 131136.

[26] Liu, X.; Gu, Y.; Sun, T.; Guo, Y.; Wei, X.; Zhao, S.; Wang, S. Water Resistant and Flexible MOF Materials for Highly Efficient Separation of Methane from Nitrogen, *Ind. Eng. Chem. Res.,* 2019, **58**, 20392-20400.

[27] Chen, Y.; Wang, Y.; Wang, Y.; Xiong, Q.; Yang, J.; Li, L.; Li, J.; Mu, B. Improving CH_4 uptake and CH_4/N_2 separation in pillar-layered metal-organic frameworks using a regulating strategy of interlayer channels, *AIChE J.,* 2022, **68**, e17819.

[28] Li, T.; Jia, X.; Chen, H.; Chang, Z.; Li, L.; Wang, Y.; Li, J. Tuning the pore environment of MOFs toward efficient CH_4/N_2 separation under humid conditions, *ACS Appl. Mater. Interfaces,* 2022, **14**, 15830-15839.

[29] Kivi, C. E.; Gelfand, B. S.; Dureckova, H.; Ho, H. K.; Ma, C.; Shimizu, G. K. H.; Woo, T. K.; Song, D. 3D Porous Metal–Organic Framework for Selective Adsorption of Methane over Dinitrogen under Ambient Pressure, *Chem. Commun.,* 2018, **54**, 14104-14107.

[30] Wu, X.; Yuan, B.; Bao, Z.; Deng, S. Adsorption of Carbon Dioxide, Methane and Nitrogen on an Ultramicroporous Copper Metal-Organic Framework, *J. Colloid Interface Sci.,* 2014, **430**, 78-84.

[31] Liu, J.; Tang, X.; Liang, X.; Wu, L.; Zhang, F.; Shi, Q.; Yang, J.; Dong, J.; Li, J. Superhydrophobic Zeolitic Imidazolate Framework with Suitable SOD Cage for Effective CH_4/N_2 Adsorptive Separation in Humid Environments, *AIChE J.,* 2022, **68**, e17589.

[32] Guo, Y.; Hu, J.; Liu, X.; Sun, T.; Zhao, S.; Wang, S. Scalable solvent-free preparation of $[Ni_3(HCOO)_6]$ frameworks for highly efficient separation of CH_4 from N_2, *Chem. Eng. J.,* 2017, **327**, 564-572.

[33] Ren, X.; Sun, T.; Hu, J.; Wang, S. Highly enhanced selectivity for the separation of CH_4 over N_2 on two ultra-microporous frameworks with multiple coordination modes, *Micropor. Mesopor. Mat.,* 2014, **186**, 137-145.

[34] Kim, T. H.; Kim, S. Y.; Yoon, T. U.; Kim, M. B.; Park, W.; Han, H. H.; Kong, C. I.; Park, C. Y.; Kim, J. H.; Bae, Y. S. Improved Methane/Nitrogen Separation Properties of Zirconium-Based Metal–Organic Framework by Incorporating Highly Polarizable Bromine Atoms, *Chem. Eng. J.,* 2020, **399**, 125717.

[35] Ma, H.; Ren, H.; Zou, X.; Meng, S.; Sun, F.; Zhu, G. Post-metalation of porous aromatic frameworks for highly efficient carbon capture from $CO_2 + N_2$ and $CH_4 + N_2$ mixtures, *Polym. Chem.,* 2014, **5**, 144-152.

[36] Saha, D.; Deng, S. Structural stability of metal organic framework MOF-177, *J. Phy. Chem. Lett.,* 2010, **1**, 73-78.

[37] Möllmer, J.; Lange, M.; Möller, A.; Patzschke, C.; Stein, K.; Lassig, D.; Lincke, J.; Glaser, R.; Krautscheid, H.; Staudt, R. Pure and mixed gas adsorption of CH_4 and N_2 on the metal–organic framework Basolite A100 and a novel copper-based 1,2,4-triazolyl isophthalate MOF, *J. Mater. Chem.,* 2012, **22**, 10274-10286.

[38] Kim, M. B.; Thallapally, P. K. Effective CH_4/N_2 Separation Using NU-1000 at High Pressures, *J. Coord. Chem.,* 2021, **74**, 216-225.

[39] Zhang, F.; Shang, H.; Zhai, B.; Li, X.; Zhang, Y.; Wang, X.; Li, J.; Yang, J. Thermodynamic-kinetic synergistic separation of CH_4/N_2 on a robust aluminum-based metal-organic framework, *AIChE J.,* 2023, **69**, e18079.